An innovative approach for characteristic analysis and state-of-health diagnosis for a Li-ion cell based on the discrete wavelet transform

Jonghoon Kim [a,*], B.H. Cho [b]

[a] Department of Electrical Engineering, Chosun University, Gwangju 501-759, Republic of Korea
[b] Power Electronics System Laboratory, School of Electrical Engineering and Computer Science, Seoul National University, Seoul 151-744, Republic of Korea

HIGHLIGHTS

- The DWT is useful for analyzing signal with non-stationary and transient phenomena.
- The discharging/charging voltage signal (DCVS) is considered as original signal.
- Daubechies dB3 wavelet is used in the multi-resolution analysis (MRA) of the DWT.
- DWT-based MRA is used to extract variable electrochemical information from the DCVS.
- The proposed work shows the clearness for reliable state-of-health (SOH) diagnosis.

ARTICLE INFO

ABSTRACT

This paper introduces an innovative approach to analyze electrochemical characteristics and state-of-health (SOH) diagnosis of a Li-ion cell based on the discrete wavelet transform (DWT). In this approach, the DWT has been applied as a powerful tool in the analysis of the discharging/charging voltage signal (DCVS) with non-stationary and transient phenomena for a Li-ion cell. Specifically, DWT-based multi-resolution analysis (MRA) is used for extracting information on the electrochemical characteristics in both time and frequency domain simultaneously. Through using the MRA with implementation of the wavelet decomposition, the information on the electrochemical characteristics of a Li-ion cell can be extracted from the DCVS over a wide frequency range. Wavelet decomposition based on the selection of the order 3 Daubechies wavelet (dB3) and scale 5 as the best wavelet function and the optimal decomposition scale is implemented. In particular, this present approach develops these investigations one step further by showing low and high frequency components (approximation component A_n and detail component D_n, respectively) extracted from variable Li-ion cells with different electrochemical characteristics caused by aging effect. Experimental results show the clearness of the DWT-based approach for the reliable diagnosis of the SOH for a Li-ion cell.

© 2014 Elsevier B.V. All rights reserved.

1. Introduction

As one of the most used batteries in consumer portable electronics in recent decades, Li-ion cells have become more and more favorable choice for portable device, power electronics, and renewable storage applications [1,2]. As a result, in these days, battery management system (BMS) of the rechargeable Li-ion cell is one of the major concerns for electric-powered transportation such as electric vehicles (EVs) and hybrid electric vehicles (HEVs)

in order to guarantee the overall system performance. Therefore, for achievement of an improved BMS, accurate and reliable knowledge of a Li-ion cell is crucial to achieve these goals [3–8]. Failure to achieve an improved BMS, leading to over-discharging and over-charging conditions, may cause permanent internal damage [9,10]. However, due to the complex chemical and physical process of the cells, the behavior of the cells show nonlinear characteristic, and thus is difficult to acquire optimal BMS. As a result, in order to overcome these weak points, the electrochemical models [11–16] and the electrical circuit models (ECMs) [17–23] have been representatively studied and applied Li-ion cell for efficient analysis cell's behavior. The electrochemical models enable an utilization of a set of coupled non-
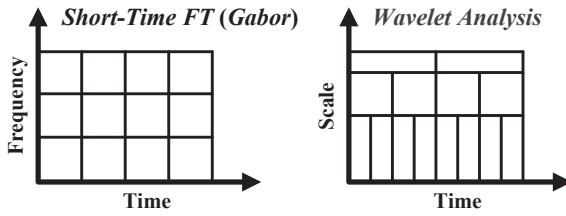
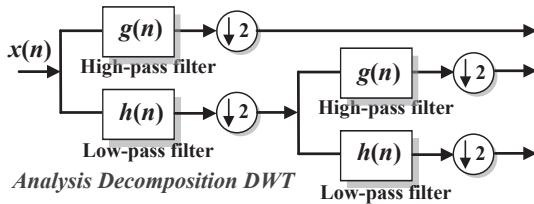**Fig. 1.** Windows functions of two signal processing transform.

Fig. 2. Discrete wavelet transform (DWT)-based multi-resolution analysis (MRA) of the signal.
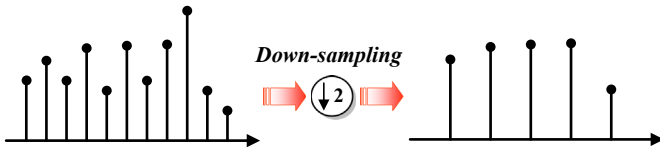

Fig. 3. Down-sampling of the DWT.

linear differential equations for description of the pertinent transport, thermo-dynamic effect, and kinetic phenomena occurring in the cell. In addition to the relationship between microscopic quantities, the distribution in the cell can be easily translated into measureable quantities (cell current and voltage). Unfortunately, the electrochemical models should accompany partial differential equations with numerous unknown parameters, which cause a huge memory requirement and a heavy burden of computation, thus these models are inappropriate to real BMS [24].

The electrical circuit models (ECMs) have been especially investigated for the purpose of BMS and energy management control of EVs and HEVs. These models are generally comprised of resistance-capacitance (RC) networks such as first-, second-, and third-order RC ladders in order to capture $I-V$ dynamical characteristics of a cell. Through physical parameterization of the ECM, the cell's behavior can be better understood. However, from the model-based state-of-charge (SOC) estimation point of view, it has been observed that difference in electrochemical characteristics due to manufacturing variability and degradation with use, result in wrong parameter values that causes erroneous SOC estimation and low BMS performance. Although the error can be temporarily reduced by repeated measurement of model parameter values, such as exercise would be very inefficient due

to time-consuming testing, costly, and labor intensive for obtaining parameter values [24–26]. Therefore, in order to reduce these shortcomings and to enhance battery management with a requirement for more accuracy and representation of the complex nonlinear electrochemical processes, there have been some approaches that deals with parameters variability of model-based SOC and state-of-health (SOH) under different experimental condition [27,28]. The authors in Ref. [27] presented a data-driven SOC and power capability estimation of lithium-ion polymer battery using multi-state joint estimator with different degradation states. The authors in Ref. [28] presented an identical data-driven multi-scale extended Kalman filtering based parameter and state estimation against different battery aging levels. Two references show the clearness for reliable SOC and SOH information with different experimental condition. Unfortunately, so far, little definitive answer has been given to this question. In addition, due to the high complexity and long run-time performance that accompanied by enhance model of sophisticated method such as above references, an heavy embedded microprocessor should be more inevitably required to provide accurate results in real-time battery application, such as real-time SOC estimation and SOH prediction. Besides, it is very time-consuming for design of SOC and SOH estimation algorithms that satisfy the optimum specification. It should be well considered how to evaluate and get a compromise in the balance of complexity and accuracy of the BMS. Therefore, in this overall perspective, without direct an electrochemical or electrical modeling of a Li-ion cell, a novel approach as one of the key technologies of the BMS should be newly discussed in order to minimize aforementioned problems in this work.

This manuscript aims to present a new approach for characteristic analysis of a Li-ion cell based on the discrete wavelet transform (DWT) with focus on minimization of the disadvantages (model-based characteristic analysis). The DWT is becoming a powerful tool for analyzing the discharging/charging voltage signal (DCVS) with a non-stationary and transients phenomena [29–46]. One of its features is multi-resolution analysis (MRA) with a vigorous function of both time and frequency localization. Through DWT-based MRA requiring filtering and down-sampling, the information on the electrochemical characteristic of a Li-ion cell can be extracted from the DCVS over a wide frequency range. During the research specifically developed for this methodology, wavelet decomposition based on the selection of the order 3 Daubechies wavelet (dB3) and scale 3 5 as the best wavelet function and the optimal decomposition scale is used to implement as mother wavelet. The DWT decomposes the DCVS into time and frequency domains and focus on short time intervals for high frequency component (detail; D_n) and on long time intervals for low frequency component (approximation; A_n). Specifically, for feature extraction of the DCVS through DWT-based MRA, approximation A_5 and D_5 components finally decomposed are considered in this work. This study particularly develops these works one step further by showing the values of the standard deviation for high and low frequency components extracted from variable Li-ion cells with
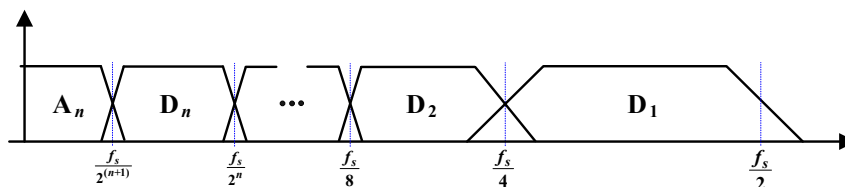

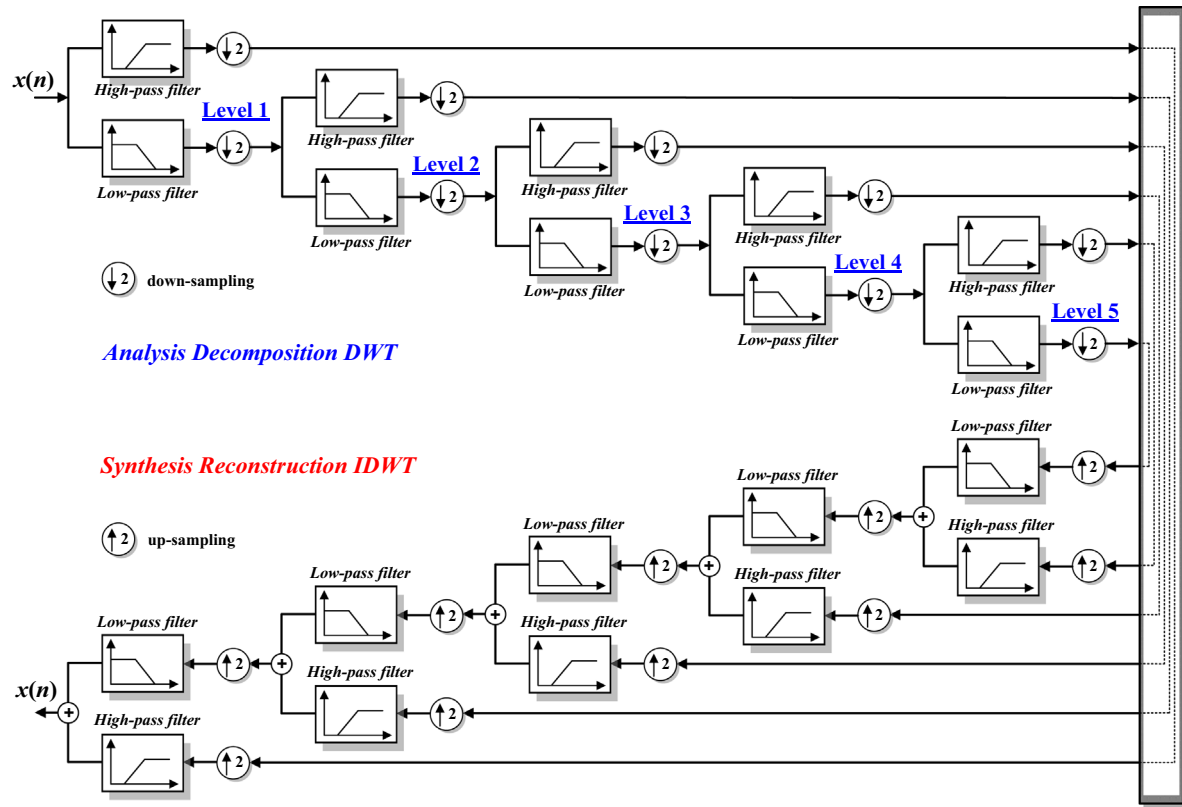**Fig. 4.** Frequency bands corresponding to the DWT signal.

Fig. 5. DWT-based decomposition and reconstruction processes with five levels.

Fig. 6. Samsung SDI 18650 LiCoO$_2$ Li-ion cell with a rated capacity (1.3 Ah).

different electrochemical characteristics caused by aging effect. Consequently, it can be shown that the experimental results clearly validated the DWT-based approach for the reliable diagnosis of the SOH. All experimental results were conducted on 18650 Li-ion cells that had a rated capacity of 1.3 Ah (Samsung SDI).

The remainder of this manuscript is organized as follows. This manuscript is divided into five parts, including this Introduction section. Section 2 shows the theoretical background on classical wavelet transform, which includes continuous wavelet transform (CWT) and DWT. Specifically, the basic introduction on the DWT-based MRA is also provided in this section. In Section 3, the experimental setup to acquire the DCVS of a Li-ion cell is described. An approach of the DWT-based characteristic analysis of a Li-ion cell is presented in Section 4. Moreover, SOH diagnosis based on the DWT-based approach and additional issues dealing with our study for EVs/HEVs applications are explained in an orderly manner. In the final section, some conclusions and final remarks are given.
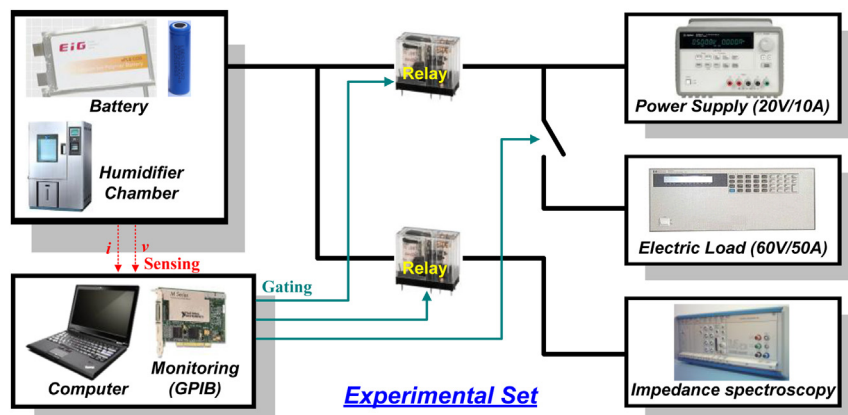

Fig. 7. Experimental setup for implementation of the proposed approach.
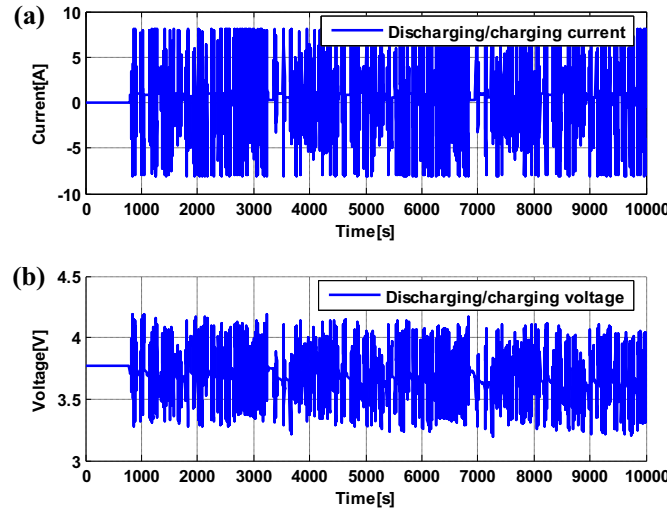
Fig. 8. Two plots for analyzing characteristics of a Li-ion cell through DWT. (a) Discharging/charging current profile (scaled-down HEV current profile). (b) Discharging/charging voltage signal data (DCVS).

2. Theoretical concept of the discrete wavelet transform (DWT)

2.1. Wavelet analysis-mathematical representation

For non-stationary signal, the Fourier analysis is not effective since it transforms the signal into the frequency domain the time information is lost. This deficiency of the Fourier analysis can be removed to some extent by analyzing a small section of the signal at a time, called as windowing. This type of analysis, known as the short-time Fourier transform (STFT) [47], however, has the drawback in that the size of the time window is the same for all frequencies. On the other hand, the wavelet transform involves a varied time-frequency window and can provide good localization property in both the frequency and time domain. Window functions of two signal processing transform are shown in Fig. 1.

Basically, a wavelet is a function $\psi(t) \in L^2(R)$ with a zero voltage.

$$\int_{-\infty}^{\infty} \psi(t)\mathrm{d}t = 0 \tag{1}$$

Then the continuous wavelet transform (CWT) of a signal $x(t)$ is defined as

$$\mathrm{CWT}\,(a,b) = \frac{1}{\sqrt{a}} \int_{-\infty}^{\infty} x(t)\psi^*\left(\frac{t-b}{a}\right)\mathrm{d}t \tag{2}$$

where $\psi(t)$ is called the mother wavelet, the asterisk denotes complex conjugate, while a and b (a, $b \in R$) are scaling (dilation and translation) parameters, respectively. The scale parameter a determines the oscillatory frequency and the length of the wavelet, and the translation parameter b determines its shifting position. During CWT analysis, the wavelet is shifted smoothly over the full domain of the analyzed signal. It thus calculates the wavelet coefficients at every scale, generating a huge amount of data. Due to the huge amount of data generated through CWT, training classifier based on its coefficients at different scales can often become cumbersome.

The DWT is derived from CWT, and its advantage is that it does not shift and scale continuously, and can only be operated in discrete steps. It also provides sufficient information and offers high reduction in the computational time. The DWT can be defined as

$$\mathrm{DWT}(a,b) = \frac{1}{\sqrt{2^j}} \int_{-\infty}^{\infty} x(t)\psi^*\left(\frac{t-k2^j}{2^j}\right)\mathrm{d}t \tag{3}$$

where a and b are replaced by 2^j and $2^j k$. This defines a dyadic-orthonormal wavelet transform and provides the basis for MRA.

2.2. DWT-based multi-resolution analysis (MRA)

In multi-resolution analysis (MRA) process, any time series $x(t)$ can be completely decomposed in terms of approximations, provided by scaling function $\phi_{j,k}(t)$ and the details, provided by the wavelet function $\psi_{j,k}(t)$, and are defined as the following:

$$\phi_{j,k}(t) = 2^{-\frac{j}{2}}\phi\left(2^{-j}t - k\right) \tag{4}$$

$$\psi_{j,k}(t) = 2^{-\frac{j}{2}}\psi\left(2^{-j}t - k\right) \tag{5}$$

where j and k are integers. The scaling function is associated with the low-pass filters with filter coefficients $h(n)$, and the wavelet function is associated with the high-pass filters with filter coefficients $g(n)$ such that $g(L-1-n) = (-1)^n h(n)$ (filter length L). These filters are constructed from the selected wavelet function
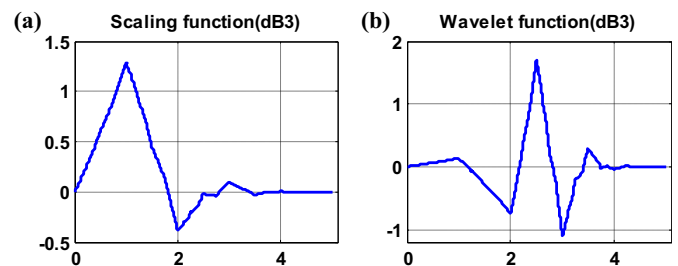

Fig. 9. Time-domain waveform of dB3 (Daubechies wavelet family). (a) Scaling function. (b) Wavelet function.

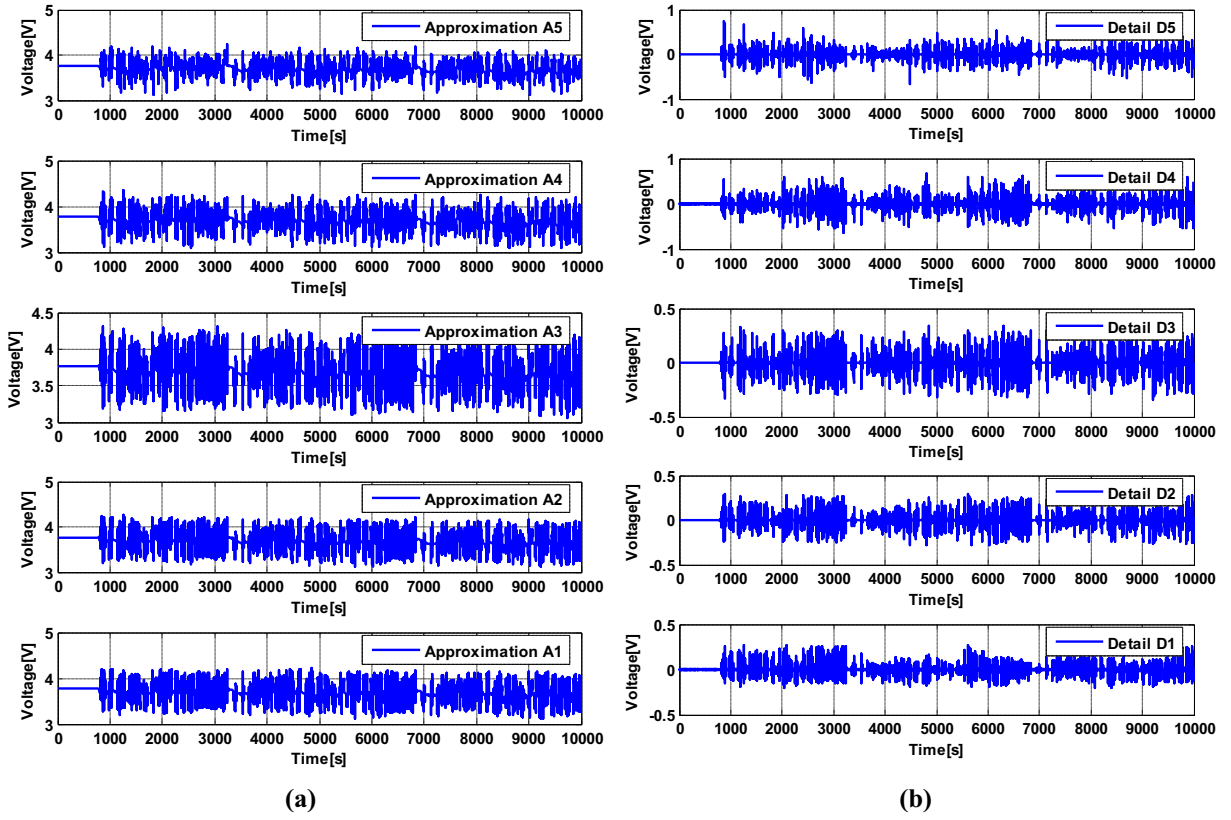**Fig. 10.** Two components through five decomposition levels of the DWT. (a) Approximation components $A_1 \sim A_5$. (b) Detail components $D_1 \sim D_5$.
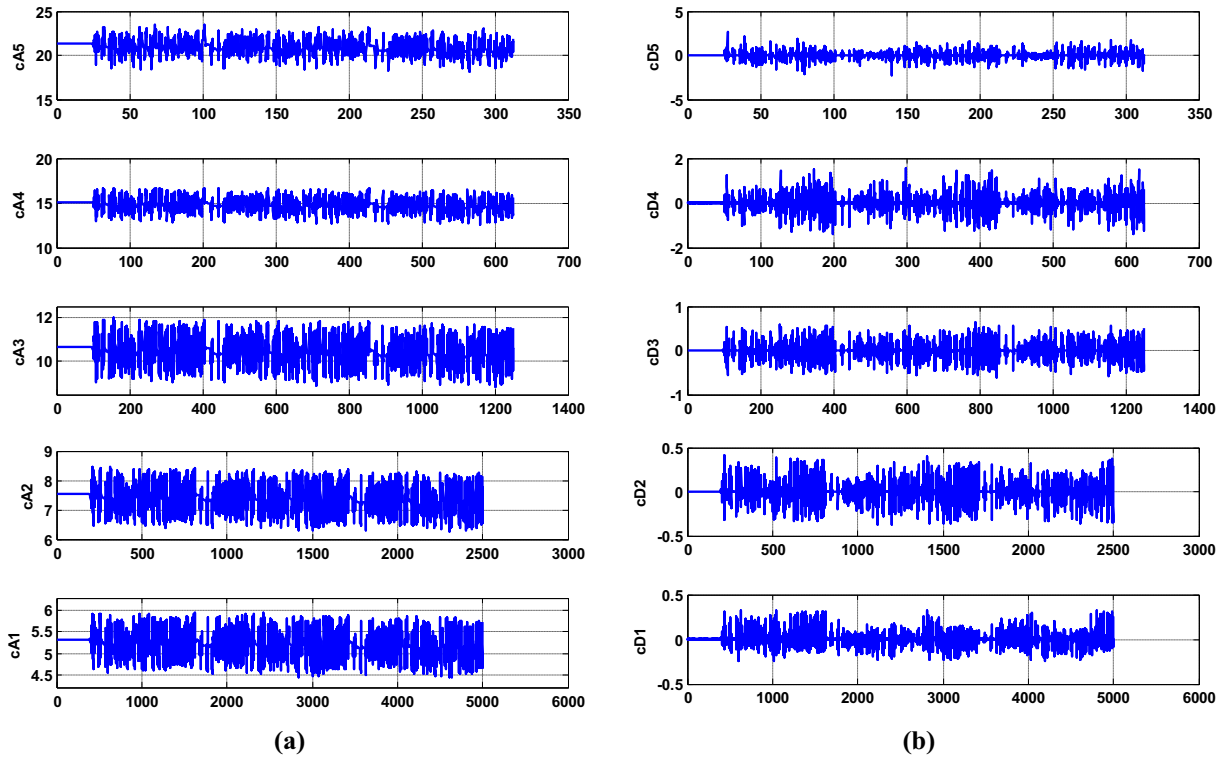

Fig. 11. Two coefficients through five decomposition levels of the DWT. (a) Approximate coefficients $a_{j,k}$ ($cA_1 \sim cA_5$). (b) Detailed coefficients $d_{j,k}$ ($cD_1 \sim cD_5$).
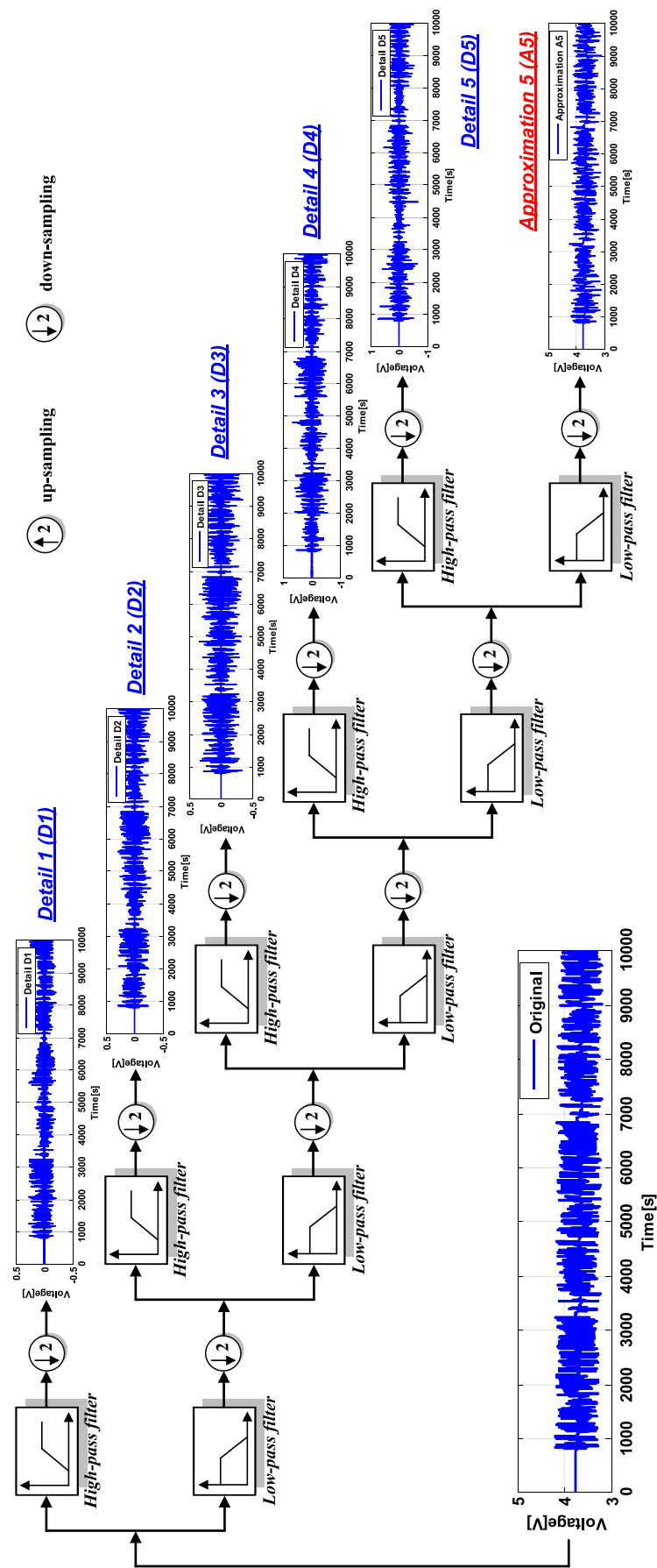
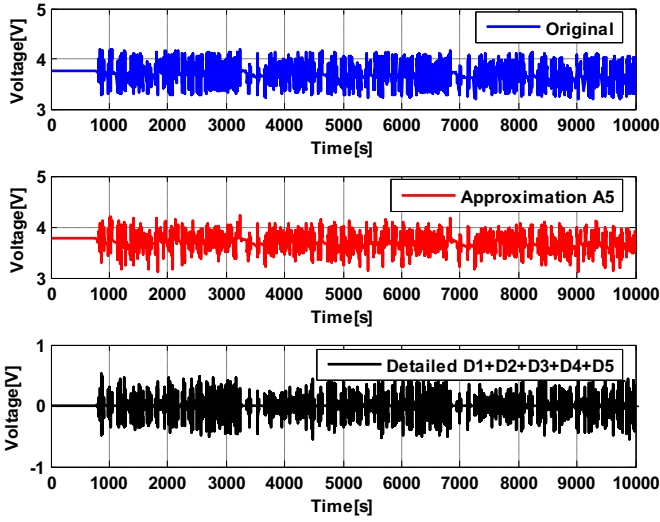**Fig. 12.** Decomposition process of the DWT-based five-level MRA.

Fig. 13. Three plots for original signal DCVS $x(t)$, approximation A_5, and detail components $D_1 \sim D_5$ through DWT-based five-level MRA.
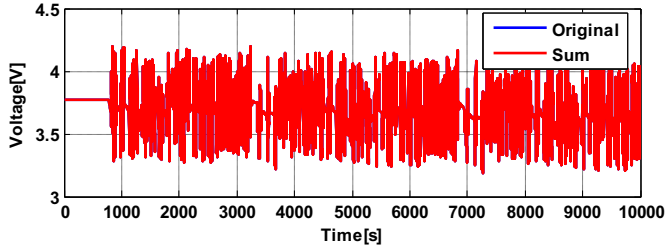

Fig. 14. Comparison between original signal DCVS $x(t)$ and the sum of six components (reconstruction; approximation A_5 and detail components $D_1 \sim D_5$).

$\psi_{j,k}(t)$ and its corresponding scaling function $\phi_{j,k}(t)$, expressed as Eqs. (6) and (7):

$$\phi_{j,k}(t) = \sqrt{2} \sum_n h(n) \phi(2t - n) \tag{6}$$

$$\psi_{j,k}(t) = \sqrt{2} \sum_n g(n) \phi(2t - n) \tag{7}$$

with $\sum h(n) = \sqrt{2}$ and $\sum g(n) = 0$. The approximations are the low-frequency components of the time series and the details are the high-frequency components. The MRA leads to a hierarchical and fast scheme. This can be completely by a set of successive filter banks as shown in Fig. 2. Considering the filter bank

Fig. 15. Low/High filters coefficients of Daubechies wavelet dB3. (a) Decomposition process. (b) Reconstruction process.

Fig. 16. Approximation A_5 and detail $D_1 \sim D_5$ components decomposed by the DWT-based five level (original signal: discharging/charging voltage with discharging current of 3 A).

implementation, the relationship of the approximation coefficients and detail coefficients between two adjacent levels are given as

$$a_{j,k} = < x(t), \phi_{j,k}(t) \geq \sum_n h(n - 2k) a_{j-1,n} \tag{8}$$

$$d_{j,k} = < x(t), \psi_{j,k}(t) \geq \sum_n g(n - 2k) a_{j-1,n} \tag{9}$$

where $a_{j,k}$ and $d_{j,k}$ represent the approximation coefficients and detail coefficients of the signal at level j, respectively. Since $x(t)$ has a length of 2^N, then there is a maximum of N levels of decomposition, or a maximum N ($J \leq N$) of applications of $h(n)$ and $g(n)$. Therefore, the J-level DWT representation of a signal $x(t)$ can be defined as Eq. (10).

Fig. 17. Two coefficients through five decomposition levels of the DWT (from Fig. 16). (a) Approximate coefficients $a_{j,k}$ ($cA_1 \sim cA_5$). (b) Detailed coefficients $d_{j,k}$ ($cD_1 \sim cD_5$).

Fig. 18. Three plots for original voltage, approximation component A_5, and detail component D_5 for direct current internal resistance (DCIR) profiles from 1 A through 6 A at the discharge region.

$$x(t) = \sum_{k=0}^{2^{N-j}-1} a_{j,k} 2^{-\frac{j}{2}} \phi\left(2^{-j}t - k\right) + \sum_{j=1}^{J} \sum_{k=0}^{2^{N-j}-1} d_{j,k} 2^{-\frac{j}{2}} \psi\left(2^{-j}t - k\right)$$
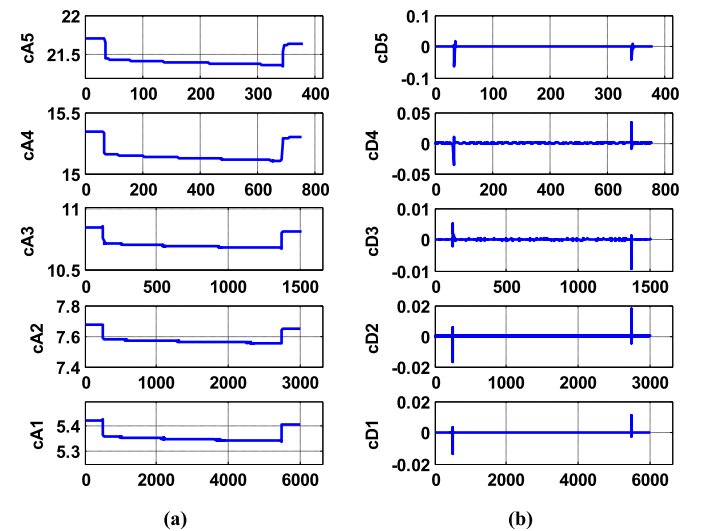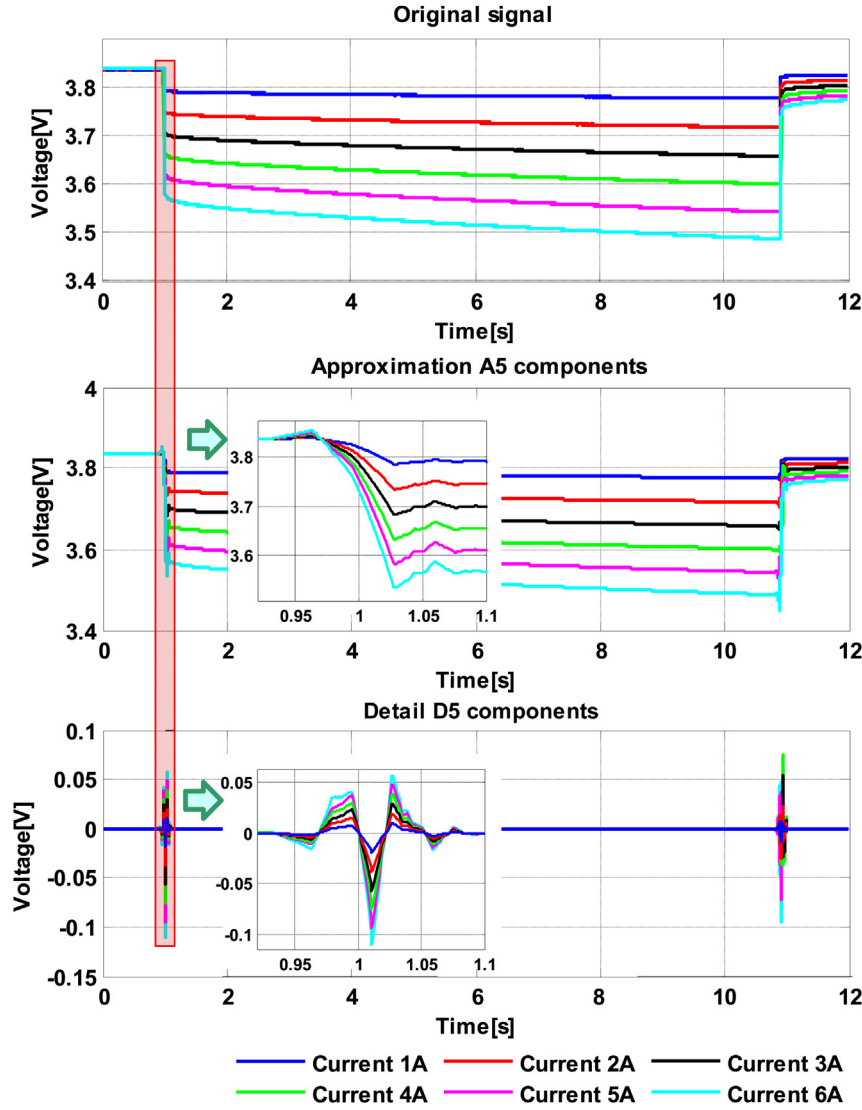
(10)

where J ($J \leq N$) is the number of levels of decomposition. Each set of wavelet transform coefficients $a_{j,k}$ and $d_{j,k}$ for $1 \leq j \leq J$, represents a band-pass filtered and down-sampled version (Fig. 3) of the original signal $x(t)$. The decomposition process can be iterated, with successive approximations being decomposed in turn, so that a signal $x(t)$ is broken down into many lower resolution components. This is called the wavelet decomposition tree. In practice, a suitable level number n is selected based on the nature of the signal, or on some other suitable criterion. Fig. 4 shows a qualitative representation of the transfer function of the filters used in the transform. The resulting frequency bands are consecutive; the limits for these bands depend on the level of the signal and on the sampling rate. For the detail D_1, the upper limit is half the sampling rate ($f_s/2$), whereas the lower limit is $f_s/4$. For a generic detail D_n, the upper limit of its frequency band coincides with the lower limit of the band of the previous detail D_{n-1}, and its bandwidth is half the

bandwidth of its previous detail. Therefore, a generic detail D_n contains the information concerning the signal components with frequencies included within the interval $[2^{-(n+1)}f_s, 2^{-n}f_s]$ Hz. On the other hand, the approximation A_n contains the low frequency
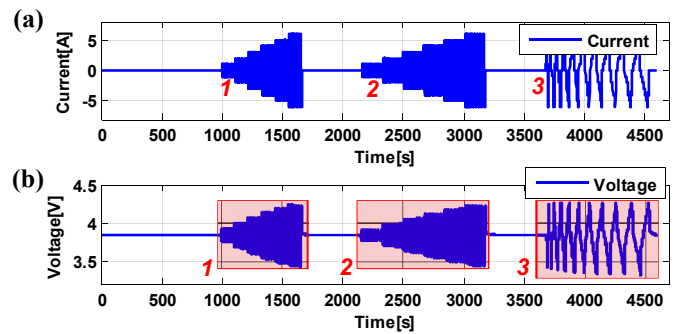

Fig. 19. Two plots for obtaining three DCVSs with different time interval, current magnitude, and abrupt changes. (a) Discharging/charging current profile. (b) Discharging/charging voltage signal data (DCVS).
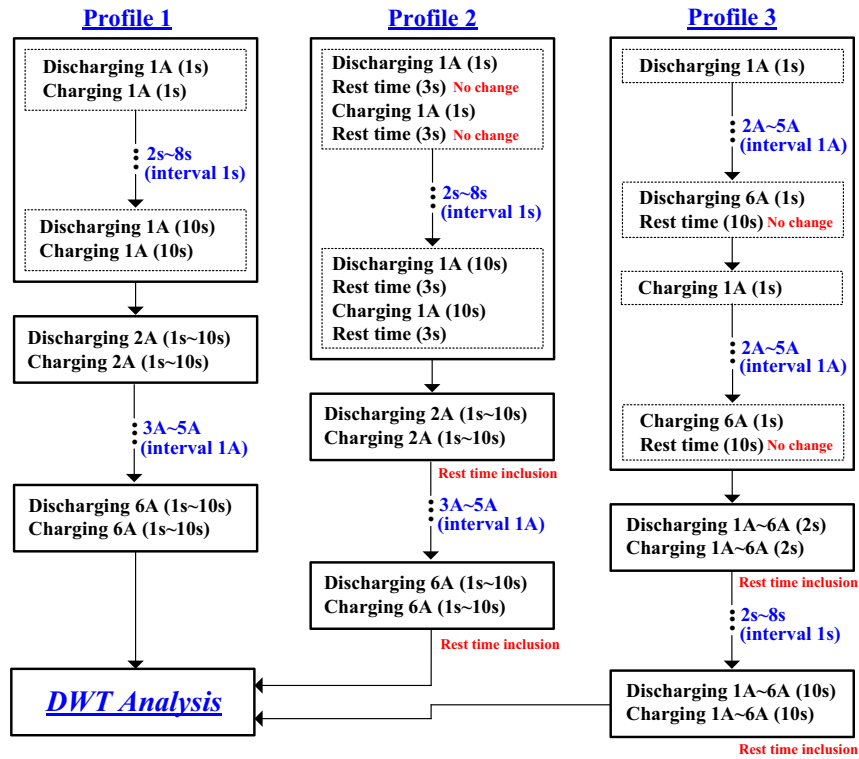
Fig. 20. Experimental procedures of three discharging/charging current profiles.

components of the original signal $x(t)$ included in the interval [0, $2^{-(n+1)}f_s$] Hz [47]. For reference, the inverse DWT (IDWT) is to reconstruct the decomposed signal $x(t)$ through the synthesis filter bank with up-sampling operations. The DWT-based decomposition and reconstruction processes are shown in Fig. 5.

3. Experimental cell and test workbench

Experimental studies were conducted on Samsung SDI 18650 LiCoO$_2$ Li-ion cells that had a rated capacity of 1.3 Ah (Fig. 6; 1S1P unit cell). The operating voltage of this cell was considered in the 2.8–4.2 V range and the nominal voltage of the cell is 3.7 V. The cell was charged at a constant current of 0.65 A (0.5C) until the voltage reached 4.2 V. Following this, a constant voltage charge maintained the voltage charge maintained the voltage at 4.2 V until the current decayed to 100 mA. In case of discharging condition, a constant current discharge at 4 A (3C) led the cell to approach the desired SOC level until fully discharged at 2.8 V. As shown in Fig. 7, the battery testing platform consisted of programmable stand-alone instruments and a computer-control unit (C++ MFC-based virtual measurement system with a PC as its platform). Stand-alone instruments are independently operated thus it support a wide variety of functions in the power and measurement field. It comprised a power supply for cell charging (Agilent E3633A), an electric load for discharging (Hewlett–Packard 6050A). The supported operating modes include the charge modes (CC–CV, CC) and the discharge modes (CC, CP, CC/CP with pulse). Predefined discharging/charging current profiles were run with the experimental test bench through a C++ MFC-based interface on a PC, which controls the power supply and electrical load and acquires measurements for a Li-ion cell. The experimental results can be precisely collected using measurement and recording system through a data acquisition board [General Purpose Interface Bus (GPIB) communication] with a high

accuracy. The recorded data include discharging/charging current, terminal voltage, SOC via Ah-counting, and temperature. Collected data is used as inputs for MATLAB/Simulink S-function simulations. BMS controller based on a self-made digital signal processor (DSP) controller using STM32F105VC for real-time control was implemented. Cell performance largely depends on ambient temperature, therefore all experimental tests were performed at 25 °C in an electronically controlled environmental/humidity chamber (Hitachi U-6652P-CH3). For reference, in order to record the cell impedance behavior at various excitation frequencies, electrochemical impedance spectroscopy (EIS) was used (Zahner IM6ex).

4. Proposed approach

4.1. Feature extraction for characteristic analysis of a Li-ion cell

An approach of the DWT-based characteristic analysis of a Li-ion cell is newly introduced. For a scaled-down discharging/charging current profile of an HEV, the experimental voltage data (DCVS) measured for 1.3 Ah Li-ion cell at 25 °C is shown in Fig. 8. The DWT is applied to the DCVS with time-frequency domain, where the different characteristics of each discharging/charging current signal appear more clearly. For analyzing and evaluating the DCVS with a non-stationary and transients, decomposition process of the MRA is implemented for extracting information from these phenomena. Fig. 8(b) as original DCVS signal $x(t)$ is passed through high and low pass filters. The filters of $h(n)$ and $g(n)$ used to decompose the original signal $x(t)$ with down-sampling and filtered coefficient vectors. The orthonormal wavelet filter of the Daubechies family that suitable for a wide range of applications is selected as the optimum wavelet function. Daubechies wavelet, which belongs to the family of orthogonal wavelets filtering a DWT, are widely used in solving a board range of problems due to its orthogonal property,
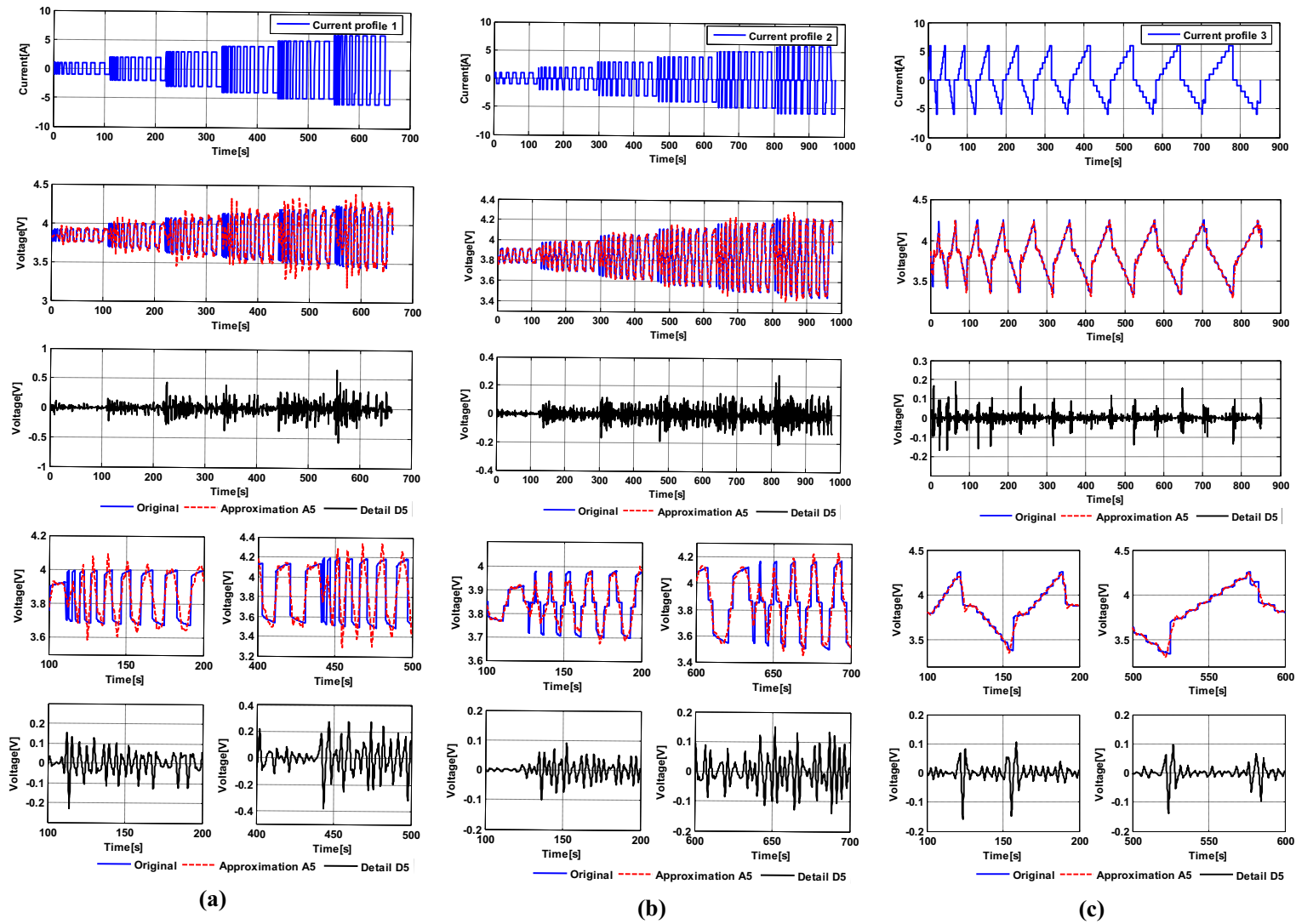
Fig. 21. Enlarged and specific experimental results to extract the features A_5 and D_5 components of the DCVS according to three current profiles. (a) Discharging/charging current profile 1. (b) Discharging/charging current profile 2. (c) Discharging/charging current profile 3.
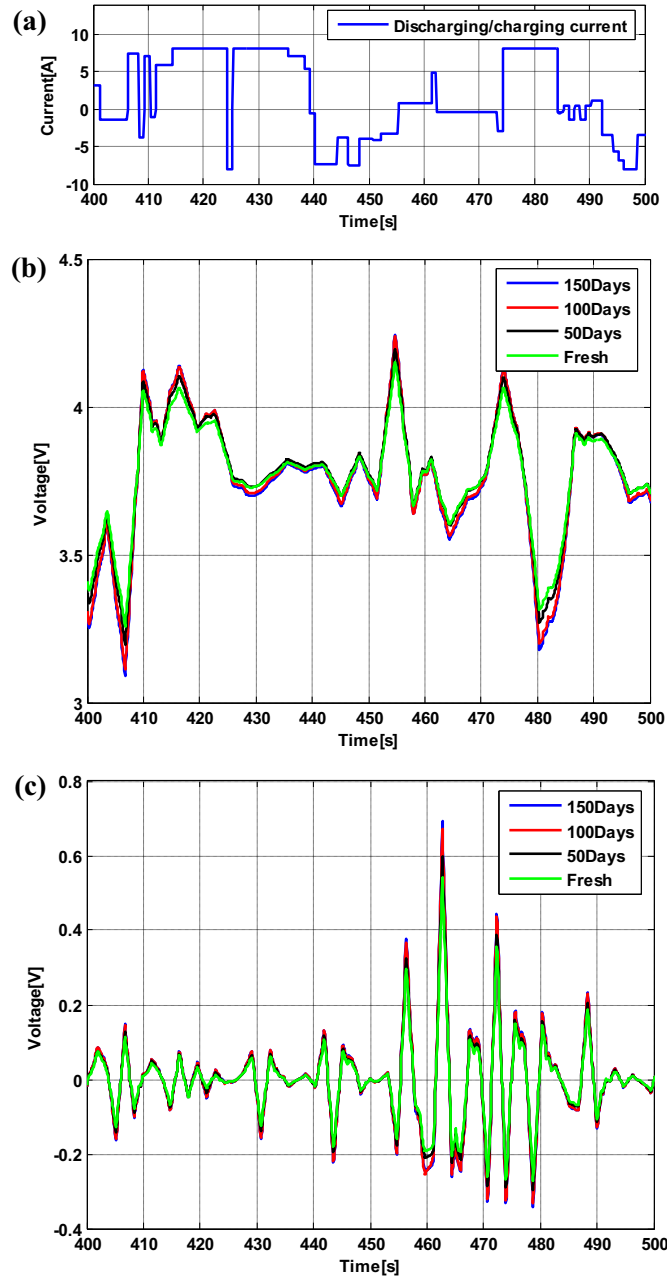
Fig. 22. Three plots for distinguishing electrochemical characteristic and state-of-health (SOH) of Li-ion cells through DWT-based MRA. (a) Discharging/charging current profile. (b) Approximation components A_5. (c) Detail components D_5.

which is potent for localization and classification of disturbance [48,49]. From viewpoint of implementation, Daubechies wavelet was selected as a good choice for the DCVS analysis. In this approach, the decomposition process, in which the Daubechies basis of order three (dB3), in five decomposition levels, has been applied to produce different frequency bands of the DCVS. Through the extracted features from all these frequency components, it is possible to obtain good discriminated results. In Fig. 9, the waveform and frequency responses of the order 3 Daubechies (dB3) scaling function and wavelet function are shown.

By down-sampling (↓2) of the MRA, the outputs from both filters are decimated to obtain two components of detail and approximation at level 1 (A_1 and D_1). Among them, the approximation component A_1 is sent to the second state to repeat this procedure

(decomposition for obtaining A_2 and D_2 at level 2). Due to five decomposition levels, it can be shown that there are each five approximation ($A_1 \sim A_5$) and detail components ($D_1 \sim D_5$) as shown in Fig. 10. Additionally, approximate $a_{j,k}$ ($cA_1 \sim cA_5$) and detailed coefficients $d_{j,k}$ ($cD_1 \sim cD_5$) which decompose to five levels by DWT are shown in Fig. 11.

For reference, the decomposition level n is selected so that detail D_n contains the frequency of the supply source f, then the approximation with the same level, A_n, only contains signal components with frequencies below f. The sampling frequency used for capturing the DCVS was $f_s = 5000$ sample s^{-1}. This sampling frequency should be considered to achieve good results it is set to an integer multiple of it. With consideration of $f = 100$ Hz, the number of decomposition levels is given by Eq. (11).
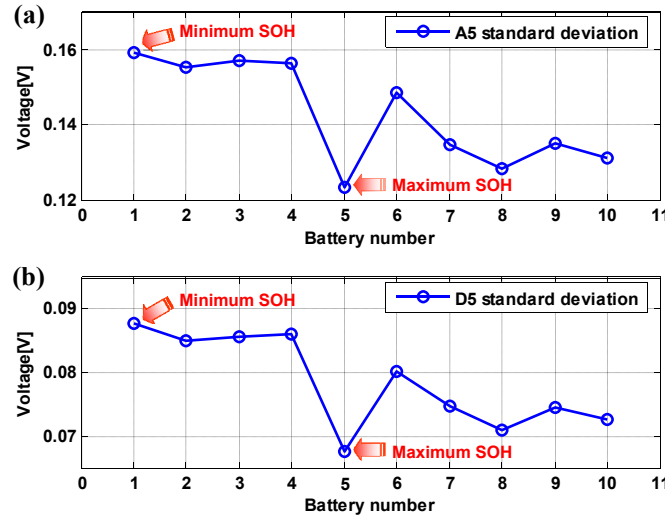
Fig. 23. Example for obtaining SOH information through standard deviations of approximation A_5 and detail D_5 components for 10 arbitrary Li-ion cells that have different electrochemical characteristics. (a) Standard deviations of 10 approximation components A_5. (b) Standard deviations of 10 detail components D_5.

$$n = \text{Integer}\left[\frac{\log(f_s/f)}{\log(2)}\right] = 5 \qquad (11)$$

The number of the data window 32, which means that the number of resolution levels can be up to five levels. As expressed in Eq. (11), the optimum number of resolution levels in the analysis was chosen to be five levels. The frequency band represented by each level depends on the number of resolution levels in addition to the sampling frequency. Applying DWT to the data window of 32 sample sizes, with sampling frequency of 5 kHz, resulted in five levels of resolutions with five approximations and details whose frequency bands are listed in Table 1.

Finally, the DCVS as original signal $x(t)$ is decomposed at the expected level. After filtering, the two components contain re-dundancies and it is valid to down-sample each of the components by a factor of two, without losing any information. According to five-level decomposition, the DCVS can be recovered in terms of sub-signals with different scale. Among all approximation ($A_1 \sim A_5$) and detail components ($D_1 \sim D_5$) by five-level MRA of the DWT, with the lowest frequency band A_5 and $D_1 \sim D_5$ with high frequency bands are selected as shown in Fig. 12 and expressed in Eq. (12).

$$x(t) = A_J + \sum_{j \leq J} D_j \left(A_{j-1} = A_j + D_j\right)$$
$$\text{At five level } x(t) = A_5 + D_1 + D_2 + D_3 + D_4 + D_5 \qquad (12)$$

where $A_j(t)$ and $D_j(t)$ express the approximation and the detailed signal of the Jth level. Three plots for original signal DCVS,

approximation component A_5 and the sum of all detailed compo-nents $D_1 \sim D_5$ through DWT-based MRA are shown in Fig. 13. Fig. 14 is additionally shown for comparison between original signal DCVS and the sum of six components (Eq. (12); approximation A_5 and detail components $D_1 \sim D_5$). It can be simply known that there is little difference between original signal and approximation component A_5. In case of the sum of detail components $D_1 \sim D_5$, it has positive or negative values with zero basis. It can be simply shown that there is little difference between original signal and approximation component A_5. For reference, as expressed in Eq. (12) and shown in Fig. 14, by the reconstruction of the inverse DWT (IDWT), it goes without saying that there is no difference between original signal $x(t)$ and reconstructed signal of approximation A_5 combined with detail components $D_1 \sim D_5$. Lower level approxi-mation and detail components combine to create higher level components with up-sampling and filtered coefficient vectors. Fig. 15 and Table 2 show the DWT filter construction showing Daubechies wavelet dB3 scaling function filter coefficients corre-sponding low-pass and high-pass filters for decomposition and reconstruction processes.

Various discharging/charging current profiles are applied to Li-ion cells in order to extract features such as current magnitude, time interval, and abrupt changes discharging/charging condition. Wavelet decomposition based of the order 3 Daubechies wavelet and scale 5 is identically applied. By predetermined scale 5, for feature extraction of the DCVS through DWT-based MRA, approx-imation A_5 and detail components D_5 finally are considered in this approach. At first, in order to analyze the DCVS characteristics with
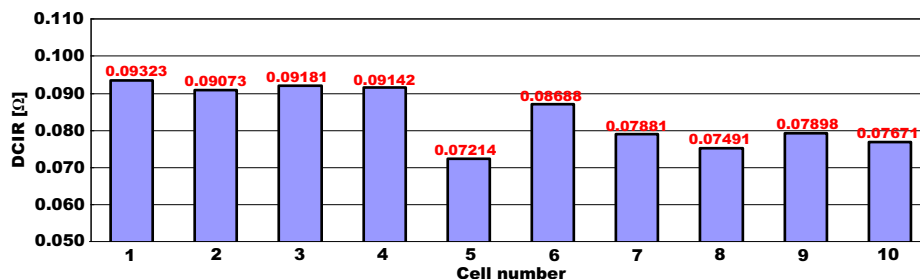

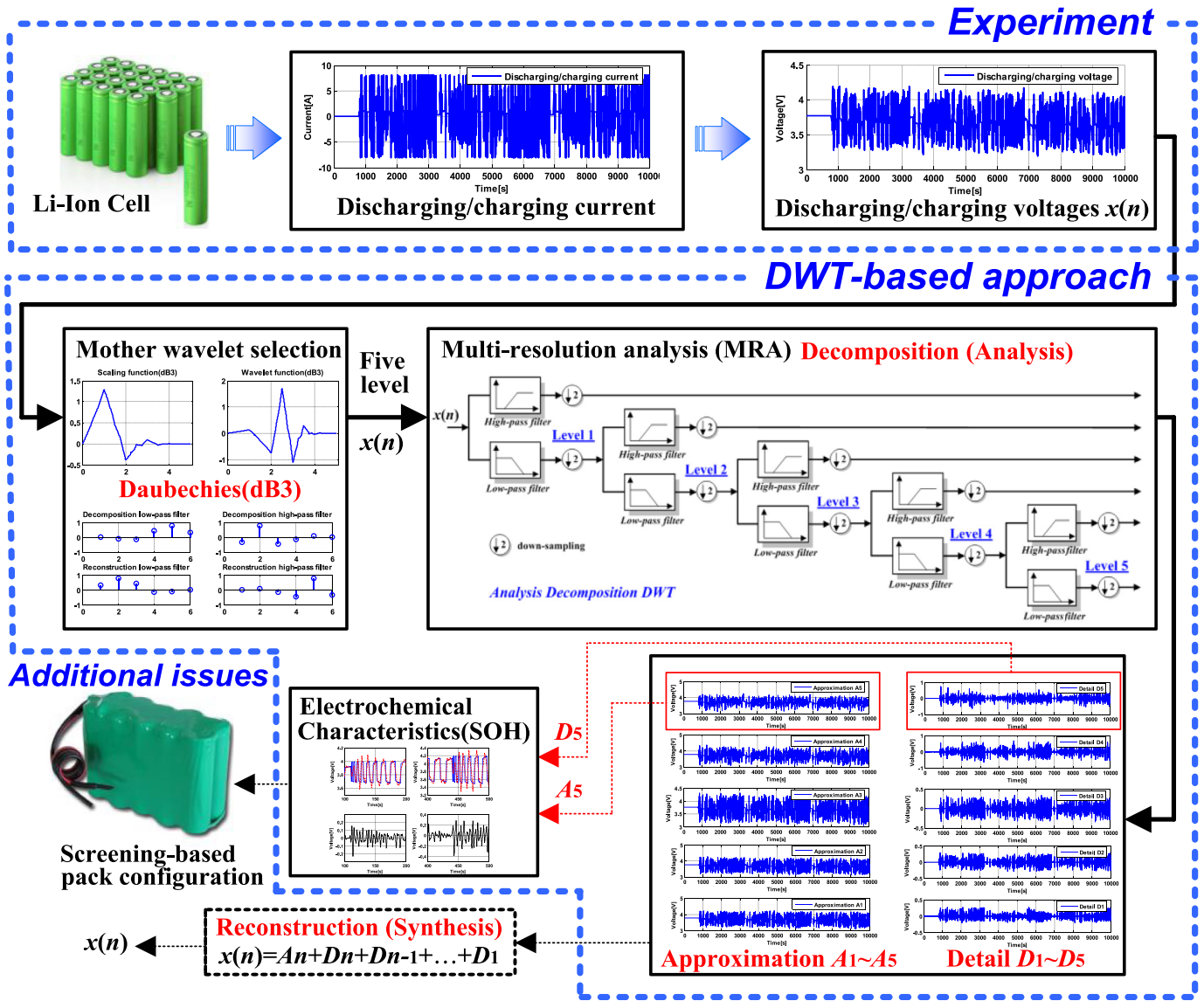**Fig. 24.** Experimental DCIR values for 10 arbitrary Li-ion cells [Ω].

Fig. 25. Schematic diagram for showing implementation process of the DWT-based approach.

current magnitude, the direct current internal resistance (DCIR) current profile [50] is simply applied to an identical Li-ion cell. After fully charging SOC 1 (100%) at a constant current of 0.65 A (0.5C), followed by a rest period (1 h), a constant current discharge at 4 A (3C) led the Li-ion cell at approach the desired SOC of 50%. After an identical period of 1 h for returning to the electrochemical equilibrium condition, the DCIR current profiles from 1 A through 6 A (interval 1 A) at the discharge region are applied during 10 s. It is made up of single repetitions (1 A through 6 A). For analyzing obtained 6 discharging voltages, decomposition process of the MRA is implemented. Fig. 16 shows the approximation A_5 and all detailed components $D_1 \sim D_5$ with discharging current of 3 A. In addition, approximate $cA_5(=a_{j,k})$ and detailed coefficients $cD_1 \sim cD_5(=d_{j,k})$ are shown in Fig. 17. Three plots for original voltage, approximation component A_5, and detail component D_5 are totally shown in Fig. 18. Due to little difference between original voltage and approximation component A_5, it can be known that electrochemical characteristics following current magnitude for original voltage and approximation component A_5 of the DWT-based MRA are approximately similar. As shown in Fig. 18, in case of the detail component D_5, it

can be specifically seen that marked difference between maximum value of absolute values (positive values) and that of absolute value (negative value) with zero basis is increased with the magnitude of current for identical discharging or charging time. Consequently, the approximation A_5 and detail components D_5 are used to analyze electrochemical characteristics with various current magnitudes applied to a Li-ion cell.

As aforementioned before, for feature extraction of the DCVS through DWT-based MRA, approximation A_5 and detail D_5 components finally decomposed are considered in this work. As shown in Fig. 19, three discharging/charging current profiles including different time interval, current magnitude, and abrupt changes are applied for obtaining each DCVSs. Each flow chart for describing experimental procedures of three discharging/charging current profiles is shown in Fig. 20. The range of all current profiles is −6 A through 6 A with an interval of 1 A. In case of the first current profile of Fig. 20(a), constant discharging and charging currents are sequentially changed and applied during 1 s through 10 s with an interval of 1 s. It is made up of single repetitions (1 A through 6 A). There is no rest between previous discharging and next charging.

Table 1
Frequency bands obtained by decomposition in multi-levels.

Level number	Wavelet decomposition	Component type	Frequency band (Hz)
1	D_1	Detail	1250–2500 ($f_s/2^2 \sim f_s/2^1$) Hz
2	D_2	Detail	625–1250 ($f_s/2^3 \sim f_s/2^2$) Hz
3	D_3	Detail	312.5–625 ($f_s/2^4 \sim f_s/2^3$) Hz
4	D_4	Detail	156.25–312.5 ($f_s/2^5 \sim f_s/2^4$) Hz
5	D_5	Detail	78.125–156.25 ($f_s/2^6 \sim f_s/2^5$) Hz
5	A_5	Approximation	0–78.125 ($0 \sim f_s/2^6$) Hz

However, as shown in Fig. 20(a) and (b), the second current profile has only rest time of 3 s between previous discharging and next charging. The third current profile of Fig. 20(c) is slightly different from Fig. 20(a) and (b). First of all, DCIR current profiles from 1 A through 6 A (interval 1 A) at the discharge regions are applied during 1 s. After 10 s for rest time, DCIR current profiles are identically applied at the charge regions. It is made up of single repetitions with duration for discharging or charging (1 s through 10 s).

Fig. 21 shows more enlarged and specific experimental results to extract the features A_5 and D_5 components of the DCVS according to three current profile's characteristics such as current magnitude, time interval, and abrupt changes discharging/charging condition. It can be known that high frequency resolution of transformed signal can detect transient better than the low frequency resolutions. It can be seen that there are a number of sharp spikes appearing immediately during the period of the transient. For long hours of discharging or charging with no change, there is little difference between original signal $x(t)$ and approximation component A_5, then the sum of detail components $D_1 \sim D_5$ is near to zero. This effectively means that all features for an original signal can be almost obtained from approximation component A_5. Abrupt change of the experimental condition of discharging/charging current profile leads to an increased sharp spike as high frequency component D_5 (discharging $\Rightarrow$ charging condition, charging $\Rightarrow$ discharging condition). Namely, through DWT-based MRA, high frequency components D_n within a small time window can be resolved, and only low frequency component A_n requires large time windows. A high frequency component D_n completes a cycle in a much shorter interval and it is possible to complete a low frequency component a cycle in a large interval. Therefore, slow and fast varying of the DCVS can be identified over long and short intervals, respectively.

4.2. State-of-health (SOH) diagnosis through DWT-based MRA

This present approach develops the DWT investigations one step further by showing approximation A_5 and detail D_5 components extracted from variable Li-ion cells with different electrochemical characteristics caused by aging effect. For this, a calendar-life test was used to degrade the Li-ion cell performance over periods of 50–150 days at 60 °C. When another current profile shown in Fig. 22(a) is applied to four Li-ion cells, each approximation A_5 and detail D_5 components are shown in Fig. 22(b) and (c), respectively. The order 3 Daubechies wavelet and scale 5 is identically applied for wavelet decomposition. It can be shown that voltage variance among four cells are clearly related to aging time, then the

magnitude of voltage variance of the cell degraded by calendar-life test during 150 days is the largest difference when compared to that of other cells. It is apparent that this difference among the cells can be effectively used as the key feature to distinguish the electrochemical characteristic and to diagnose SOH from the approximation A_5 and detail D_5 components. Therefore, through statistical analysis of standard deviation considering voltage variance, it is possible to diagnose SOH of an arbitrary Li-ion cell. For reference, Fig. 23 shows the example for obtaining SOH information through standard deviations of approximation A_5 and detail D_5 components for 10 arbitrary Li-ion cells that have different electrochemical characteristics. As shown in this figure, the cells with the largest or smallest values indicate the minimum or maximum SOH information in battery group, respectively. Finally, the SOH can be diagnosed as follows:

$$\text{SOH}_{\text{arbitrary}} = \frac{\left|\frac{A_5^{\text{curr}}-A_5^{\text{aged}}}{A_5^{\text{fresh}}-A_5^{\text{aged}}}\right| + \left|\frac{D_5^{\text{curr}}-D_5^{\text{aged}}}{D_5^{\text{fresh}}-D_5^{\text{aged}}}\right|}{2} = \frac{\text{SOH}_{A_5} + \text{SOH}_{D_5}}{2} \quad (13)$$

where A_5^{curr} and D_5^{curr} are the standard deviation of approximation A_5 detail D_5 components for an arbitrary Li-ion cell respectively, $A_5^{\text{fresh}}(D_5^{\text{fresh}})$ and $A_5^{\text{aged}}(D_5^{\text{aged}})$ are each standard deviations approximation A_5 detail D_5 components for fully fresh and aged Li-ion cells in 1.3 Ah cell group. For reference, the fully fresh cell has the largest SOH (lowest direct current internal resistance (DCIR) and voltage variance). On the other hand, the fully aged cell has the smallest SOH (largest SOH and voltage variance). Experimental DCIR values at SOC 50% for 10 Li-ion cells are shown in Fig. 24. Pulse power-based SOH prediction of an arbitrary Li-ion cell is generally implemented using obtained DCIR value. As shown in Fig. 24, it has been found that the overall trend of change between DCIR among 10 Li-ion cells is approximately similar with those of approximation A_5 and detail D_5 components. Therefore, it is possible to obtain SOH information of an arbitrary Li-ion cell using only approximation A_5 and detail D_5 components.

As expressed in Eq. (13), a final SOH of an arbitrary Li-ion cell is the average of SOH_{A_5} and SOH_{D_5} which represent SOH information for approximation A_5 and detail D_5 components, respectively. According to the values of standard deviation of A_5 and D_5 components, 10 Li-ion cells have each standard deviation of A_5 and D_5 components within these ranges of 0.1234–0.1593 V and 0.0676–0.0877 V, respectively. With obtained standard deviation values of A_5 and D_5 components (0.1404 V and 0.0769 V) for an arbitrary Li-ion cell, three values of SOH_{A_5}, SOH_{D_5}, and diagnosed SOH are expressed in Eq. (14) through (16), respectively.

$$\text{SOH}_{A_5} = \left|\frac{A_5^{\text{curr}} - A_5^{\text{aged}}}{A_5^{\text{fresh}} - A_5^{\text{aged}}}\right| = \left|\frac{0.1404 - 0.1593}{0.1234 - 0.1593}\right| \approx 0.5264 \quad (14)$$

$$\text{SOH}_{D_5} = \left|\frac{D_5^{\text{curr}} - D_5^{\text{aged}}}{D_5^{\text{fresh}} - D_5^{\text{aged}}}\right| = \left|\frac{0.0769 - 0.0877}{0.0676 - 0.0877}\right| \approx 0.5373 \quad (15)$$

Table 2
DWT filter construction showing Daubechies wavelet dB3 scaling function filter coefficients corresponding low-pass and high-pass filters for decomposition and reconstruction processes.

	Low-pass filter coefficients	High-pass filter coefficients
Decomposition	0.0352, −0.0854, −0.1350, 0.4599, 0.8069, 0.3327	−0.3327, 0.8069, −0.4599, −0.1350, 0.0854, 0.0352
Reconstruction	0.0332, 0.8069, 0.4599, −0.1350, −0.0854, 0.0352	0.0352, 0.0854, −0.1350, −0.4599, 0.8069, −0.3327

$$\text{SOH}_{\text{arbitrary}} = \frac{\text{SOH}_{A_5} + \text{SOH}_{D_5}}{2} = \frac{0.5264 + 0.5373}{2} = 0.5318$$

$$(16)$$

It is determined that the range of SOH is from 0 to 1, where 1 means that the Li-ion cell is totally healthy, or it is new, and 0 means the Li-ion cell cannot meet the power demand of the battery group. For reference, according to total number of experimental cells, diagnosed SOH range may be changed. Because, it is reasonably certain the two values of SOH_{A_5} and SOH_{D_5} for fully fresh cell and fully aged cell will be changed. For example, if there are 30 arbitrary Li-ion cells in cell group, the cells with the largest and smallest $A_5^{\text{fresh}}(D_5^{\text{fresh}})$ and $A_5^{\text{aged}}(D_5^{\text{aged}})$ can be used as fully fresh cell and fully aged cell, respectively.

4.3. Additional issues considering DWT-based approach for EVs/HEVs applications

According to the proposed approach, elaborate information on electrochemical analysis for a Li-ion cell can be provided. It is possible to develop this approach one step further by showing additional issues for EVs/HEVs applications. For electric-powered transportation of EVs/HEVs, multiple cells are generally assembled together in three configurations of series, parallel, and series/parallel to satisfy the high voltage/energy requirements [51–54]. Unfortunately, because of degradation with use, manufacturing variability, and cell architecture, it has been observed that individual cells in a real pack will typically show some variation, namely cell-to-cell variation, in performance depending on the specific operating condition [55,56]. Inhomogeneity among cells leads to dissimilarity in certain properties of the cells and results in performance variation. The non-uniformity observed in cell voltages may limit the maximum output of the battery pack. Therefore, on the pack level, the needs for identification and equalization of cell variations are importantly considered as critical issues for EVs/HEVs battery packs safety and efficiency.

Various ways for equalization circuits have been widely investigated and used to protect against abrupt failures to extend cell's life [57–59]. However, there are some inevitable limitations for overcoming cell-to-cell variations. Firstly, it is expected to be cost more expensive and sizing-increasing for achievement of the sophisticated equalization topology. Secondly, these equalizers cannot absolutely guarantee SOC matching among the single cells, together with voltage matching. Thirdly, even though information on voltages and SOCs of the cells in the pack are approximately similar through voltage/SOC equalizers, it is inevitable that voltage/SOC mismatching in the battery pack certainly reoccurred following the discharging/charging current applied to the battery pack. Therefore, without equalization techniques, a novel approach should be investigated to alleviate the problem of non-uniformity caused by cell-to-cell variation because of electrochemical characteristics difference.

Screening process is to select that have similar electrochemical characteristics within a cell group. Conventional method [60] implemented two kinds of screening processes, such as discharge capacity screening and resistance screening in an orderly manner. The cells finally selected are used to configure variable battery packs with safety. Using these packs, Ref. [60] describes an effort to provide each equivalent circuit model for multi-cell battery strings in series, parallel, and series/parallel connections. Simplified model-based SOC estimation using extended Kalman filter (EKF) [60,61] enables us to provide significant SOC improvement with high accuracy.

Through using DWT-based approach, it is more expected to obtain elaborate and useful information on electrochemical characteristics than conventional method of Ref. [60]. Above all,

discharging/charging voltage with non-stationary and transient phenomena can be effectively analyzed. Besides, DWT-based MRA is used for extracting information on the electrochemical characteristics in both time and frequency domain simultaneously. By additional statistical analyses including average, standard deviation, and maximum/minimum values of the low and high frequency components, cell's similarity accuracy of screening process can be increased. The BMS controller applied for real-time control such as cell voltage/current sensing, pack total voltage sensing, and relay control, is additionally used to perform statistical analysis. For reference, in the proposed approach, BMS controller based on self-made DSP controller using STM32F105VC is implemented. Stable configuration of the battery pack based on screening process is really attractive for EVs/HEVs manufactures. Besides, outstanding results of model-based SOC estimation and SOH prediction can be expected to provide en efficient EVs/HEVs operation with optimum BMS. In the light of these considerations, DWT-based approach is absolutely necessary and indispensable part of car industry. The schematic diagram that depicts implementation process of the proposed approach including additional issues for EVs/HEVs applications is displayed in Fig. 25.

5. Conclusion

Accurate and reliable knowledge of the Li-ion cell is absolutely necessary to satisfy for an improved BMS. Nowadays, the electrochemical models and ECMs have been representatively researched and applied Li-ion cell. However, in case of the electrochemical models, due to difficulty in implementing of partial differential equations with numerous unknown parameters, these models are inappropriate to real BMS. RC-network based ECMs enables us to capture $I-V$ dynamical characteristics of a Li-ion cell. Unfortunately, it is inevitable that difference in electrochemical characteristics due to manufacturing variability and degradation with use, result in wrong parameter values that causes erroneous SOC estimation and low BMS performance. Thus, in order to minimize aforementioned problems of electrochemical models and ECMs, a novel approach should be absolutely discussed.

This research deals with an innovative approach to analyze electrochemical characteristics and SOH diagnosis of a Li-ion cell based on the discrete wavelet transform (DWT). The DCVS with non-stationary and transient phenomena is applied as original voltage $x(t)$ of DWT. Specifically, in order to extract information on the electrochemical characteristics in both time and frequency domain simultaneously from the DCVS, DWT-based MRA is applied. As a result, through using the MRA with implementation of the wavelet decomposition (order 3 Daubechies wavelet (dB3) and scale 5), it is possible to extract the information on the electrochemical characteristics over a wide frequency range. This research particularly develops these investigations one step further by showing low frequency component (approximation A_n) and high frequency component (detail D_n) extracted from variable Li-ion cells with different electrochemical characteristics caused by aging effect. Experimental results show the robustness of the DWT-based approach for the reliable SOH diagnosis for a Li-ion cell.

Nomenclature

EVs/HEVs electric vehicles/hybrid electric vehicles
SOC   state-of-charge
SOH   state-of-health
BMS   battery management system
CWT   continuous wavelet transform
DWT   discrete wavelet transform
MRA   multi-resolution analysis
DCVS   discharging/charging voltage signal

A_n	approximation component
D_n	detail component
$\phi_{j,k}(t)$	scaling function of the signal at level j
$\psi_{j,k}(t)$	wavelet function of the signal at level j
$a_{j,k}$	approximation coefficients of the signal at level j
$d_{j,k}$	detail coefficients of the signal at level j
$h(n)$	filter coefficient of the low-pass filters
$g(n)$	filter coefficient of the high-pass filters
J	decomposition level
N	maximum of the decomposition level
CC	constant current
CV	constant voltage
CP	constant power
DCIR	direct current interval resistance

References

[1] J.P. Schmidt, P. Berg, M. Schönleber, A. Weber, E. Ivers-Tiffée, J. Power Sources 221 (2013) 70–77.
[2] L. Hu, Z. Zhang, K. Amine, J. Power Sources 236 (2013) 175–180.
[3] A. Manenti, A. Abba, A. Merati, S.M. Savaresi, A. Geraci, IEEE Trans. Ind. Electron. 58 (9) (2011) 4314–4322.
[4] Z. Chen, Y. Fu, C.C. Mi, IEEE Trans. Veh. Technol. 62 (3) (2013) 1020–1030.
[5] J. Kim, S. Lee, B.H. Cho, J. Power Sources 196 (2011) 2227–2240.
[6] J. Kim, S. Lee, B.H. Cho, IEEE Trans. Power Electron. 27 (1) (2012) 436–451.
[7] X. Long, W. Junping, C. Quanshi, Energy Convers. Manage. 53 (2012) 33–39.
[8] J. Kim, B.H. Cho, IEEE Trans. Veh. Technol. 60 (9) (2011) 4249–4260.
[9] J. Kim, J. Shin, C. Chun, B.H. Cho, IEEE Trans. Power Electron. 27 (1) (2012) 411–424.
[10] L. Lu, X. Han, J. Li, J. Hua, M. Ouyang, J. Power Sources 226 (2013) 272–288.
[11] M. Guo, G.-H. Kim, R.E. White, J. Power Sources 240 (2013) 80–94.
[12] X. Hu, S. Stanton, L. Cai, R.E. White, J. Power Sources 214 (2012) 40–50.
[13] L. Cai, Y. Dai, M. Nicholson, R.E. White, K. Jagannathan, G. Bhatia, J. Power Sources 221 (2013) 191–200.
[14] K.A. Smith, C.D. Rahn, C.Y. Wang, IEEE Trans. Control Syst. Technol. 18 (3) (2010) 654–663.
[15] K.-H. Xue, G.L. Plett, Electrochim. Acta 87 (2013) 575–590.
[16] Y. Hu, S. Yurkovich, Y. Guezennec, B.J. Yurkovich, J. Power Sources 196 (2011) 449–457.
[17] X. Hu, S. Li, H. Peng, J. Power Sources 198 (2012) 359–367.
[18] K.S. Hariharan, J. Power Sources 222 (2013) 210–217.
[19] T. Hu, H. Jung, J. Power Sources 233 (2013) 14–22.
[20] M.R. Mohamed, H. Ahmad, M.N.A. Seman, S. Razali, M.S. Najib, J. Power Sources 239 (2013) 284–293.
[21] Y. Hu, S. Yurkovich, J. Power Sources 196 (2011) 2913–2923.
[22] S. Bhide, T. Shim, IEEE Trans. Veh. Technol. 60 (3) (2011) 819–829.
[23] T. Osaka, T. Momma, D. Mukoyama, H. Nara, J. Power Sources 205 (2012) 483–486.
[24] H. He, R. Xiong, H. Guo, S. Li, Energ. Convers. Manage. 64 (2012) 113–121.
[25] T. Kim, W. Qiao, IEEE Trans. Energy Convers. 26 (4) (2011) 1172–1180.
[26] C. Antaloae, J. Marco, F. Assadian, IEEE Trans. Veh. Technol. 61 (9) (2012) 3881–3892.
[27] R. Xiong, F. Sun, H. He, T. Nguyen, Energy 63 (2013) 295–308.
[28] R. Xiong, F. Sun, Z. Chen, H. He, Appl. Energy 113 (2014) 463–476.
[29] M. Riera-Guasp, J.A. Antonino-Daviu, M. Pineda-Sanchez, R. Puche-Panadero, J. Perez-Cruz, IEEE Trans. Ind. Electron. 55 (12) (2008) 4167–4180.
[30] K.L.V. Iyer, X. Lu, Y. Usama, V. Ramakrishnan, N.C. Kar, IEEE Trans. Ind. Electron. 60 (4) (2013) 1638–1651.
[31] Y. Ates, O. Erdinc, M. Uzunoglu, B. Vural, Int. J. Hydrogen Energy 35 (2010) 774–783.
[32] O. Erdinc, B. Vural, M. Uzunoglu, J. Power Sources 194 (2009) 369–380.
[33] C. Arizmendi, A. Vellido, E. Romero, Expert Syst. Appl. 39 (2012) 5223–5232.
[34] X. Zhang, C.C. Mi, A. Masrur, D. Daniszewski, J. Power Sources 185 (2008) 1533–1543.
[35] P. Zheng, J. Huang, IEEE Trans. Image Process. 22 (6) (2013) 2455–2468.
[36] R.C. Guido, Appl. Math. Lett. 24 (2011) 1257–1259.
[37] C. Vonesch, T. Blu, M. Unser, IEEE Trans. Signal Process. 55 (9) (2007) 4415–4429.
[38] A.A. Hossam Eldin, M.A. Refaey, Electric Power Syst. Res. 81 (2011) 19–24.
[39] P.L. Mao, R.K. Aggarwal, IEEE Trans. Power Delivery 16 (4) (2001) 654–660.
[40] N. Saravanan, K.I. Ramachandran, Electric Power Syst. Res. 81 (2011) 19–24.
[41] R. Yan, R.X. Gao, X. Chen, Signal Process. 96 (2014) 1–15.
[42] S. Avdakovic, A. Nuhannovic, M. Kusljugic, M. Music, Electric Power Syst. Res. 83 (2012) 237–245.
[43] Y. Song, L. Gao, IEEE Trans. Comp. Pack. Man. 1 (7) (2011) 1075–1081.
[44] M.A.S.K. Khan, M.A. Rahman, IEEE Trans. Ind. Appl. 47 (5) (2011) 2241–2249.
[45] S.H. Kia, H. Henao, G.-A. Capolino, IEEE Trans. Ind. Appl. 45 (4) (2009) 1395–1404.
[46] B. Chen, Z. Zhang, C. Sun, B. Li, Y. Zi, Z. He, Mech. Syst. Signal Process. 33 (2012) 275–298.
[47] A. Bouzida, O. Touhami, R. Ibtiouen, A. Belouchrani, M. Fadel, A. Rezzoug, IEEE Trans. Ind. Electron. 58 (9) (2011) 4385–4395.
[48] A.Y. Goharrizi, N. Sepehri, IEEE Trans. Ind. Electron. 57 (5) (2010) 1755–1763.
[49] C. Sen, Y. Usama, T. Carciumaru, X. Lu, N.C. Kar, IEEE Trans. Smart Grid 3 (1) (2012) 422–433.
[50] J.-H. Kim, S.-J. Lee, J.-M. Lee, B.H. Cho, in: IEEE International Conference Power Electronics (ICPE), 2007, pp. 1173–1178.
[51] M. Uno, K. Tanaka, IEEE Trans. Ind. Electron. 60 (8) (2013) 3227–3239.
[52] A. Chaouachi, R.M. Kamel, R. Andoulsi, K. Nagasaka, IEEE Trans. Ind. Electron. 60 (4) (2013) 1688–1699.
[53] S. Chopra, P. Bauer, IEEE Trans. Ind. Electron. 60 (1) (2013) 329–338.
[54] P. Muñoz-Condes, M. Gomez-Parra, C. Sahcho, M.A.G.S. Andrés, F.J. González-Fernández, J. Carpio, R.U. Guirado, IEEE Trans. Ind. Electron. 60 (7) (2013) 2750–2759.
[55] Y. Zheng, M. Ouyang, L. Lu, J. Li, X. Han, L. Xu, H. Ma, T.A. Dollmeyer, V. Freyermuth, Appl. Energy 111 (2013) 571–580.
[56] C. Hu, B.D. Youn, J. Chung, Appl. Energy 92 (2012) 694–704.
[57] J. Gallardo-Lozano, E. Romero-Cadaval, M.I. Milanes-Montero, M.A. Guerrero-Martinez, J. Power Sources 246 (2014) 934–949.
[58] Y. Zheng, M. Ouyang, L. Lu, J. Li, X. Han, L. Xu, J. Power Sources 247 (2014) 676–686.
[59] C.-S. Lim, K.-J. Lee, N.-J. Ku, D.-S. Hyun, R.-Y. Kim, IEEE Trans. Power Electron. 29 (4) (2014) 1791–1799.
[60] J. Kim, B.H. Cho, Energy 57 (2013) 581–599.
[61] M. Charkhgard, M. Farrokhi, IEEE Trans. Ind. Electron. 57 (12) (2010) 4178–4187.